Consolidation of building materials with a phosphate-based treatment: effects on the microstructure and on the 3D pore network

Elena Possenti [a, *], Chiara Colombo [a], Claudia Conti [a], Nicoletta Marinoni [b], Marco Merlini [b], Riccardo Negrotti [a], Marco Realini [a], G. Diego Gatta [b]

[a] *Istituto per la Conservazione e la Valorizzazione dei Beni Culturali (ICVBC), Consiglio Nazionale delle Ricerche (CNR), Via R. Cozzi 53, 20125 Milano, Italy*

[b] *Dipartimento di Scienze della Terra, Università degli Studi di Milano, Via S. Botticelli 23, 20133 Milano, Italy*

**** Corresponding author: possenti@icvbc.cnr.it, Phone number: +39 02 66173386***

E-mail addresses: possenti@icvbc.cnr.it (E. Possenti, ORCID 0000-0002-9041-7971), c.colombo@icvbc.cnr.it (C. Colombo, ORCID 0000-0003-2735-539X), c.conti@icvbc.cnr.it (C. Conti, ORCID 0000-0002-5379-7995), nicoletta.marinoni@unimi.it (N. Marinoni, ORCID 0000-0003-4969-4923), marco.merlini@unimi.it (M. Merlini, ORCID 0000-0002-1146-2468), negrotti@icvbc.cnr.it (R. Negrotti, ORCID 0000-0003-1453-4823) m.realini@icvbc.cnr.it (M. Realini, ORCID 0000-0002-7212-3806), diego.gatta@unimi.it (G. D. Gatta, ORCID 0000-0001-8348-7181)

Abstract

Inorganic-mineral treatments are commonly applied to decayed stone substrates in order to slow down the decay processes, through the partial transformation of the original stone material of the substrate into newly-formed crystalline phases. The purpose of this study is to explore the effects induced by a promising consolidating treatment based on diammonium hydrogenphosphate (DAP) solutions on Noto limestone, a porous carbonatic matrix used as ornamental stone in the south of Italy. The research findings, obtained combining water absorption by capillarity measurements, mercury intrusion porosimetry (MIP) and synchrotron radiation X-ray micro-computed tomography (SR-μCT), demonstrate that the DAP consolidation induces apparent microstructural modifications of the stone in terms of

porosity and pore size distribution, changing the capillarity absorption values and decreasing the sorptivity speed. This study paves the way to a deeper investigation of the effects induced by a wider range of conservation treatments to the 3D microstructural features of porous geomaterials, by using an innovative multi-scale approach.

Keywords:

Synchrotron radiation X-ray micro-computed tomography; natural stone material; inorganic consolidant; Cultural Heritage; mercury intrusion porosimetry

Note for the print:

All the figures can be printed in black and white in the paper print of the research article. Colours can be used in the digital version of the article.

1 Introduction

The carbonatic stones used in buildings and sculptures are particularly sensitive to the action of the atmospheric agents, especially when carved and exposed in polluted urban environments. Over time, these ornamental materials are affected by decay processes, leading to decohesion and loss of material [1,2]. Consolidating treatments are commonly applied on the stone surface to slow down the decay process and to restore the loss cohesion among detached stone grains. In the wide scenario of available treatments for carbonatic stones, the inorganic-mineral diammonium hydrogenphosphate (DAP) is considered one of the most promising [3–8].

The DAP treatment, when applied in the form of water-based solutions to carbonatic matrixes, penetrates inside the pores of the stone material, reacts with the substrate and forms newly-formed phases directly within the stone matrix. It is reasonable to suppose that the crystallization of these new phases leads to the modification of some of the properties of the lithotype, *e.g.*, microstructure, porosity and sorptivity. SEM and thin-section study under transmitting-light microscope [9] are widely used methods for assesing the modifications

induced by the consolidants to the stones, while physical and mechanical standard tests (UNI EN 15886 [10], UNI EN 15801 [11], NORMAL 7/81 [12], NORMAL 29/88 [13], DRMS [14]) are usually applied to evaluate the induced effects. Furthermore, the coupling of these techniques with the mercury intrusion porosimetry (MIP) and the capillarity measurements enriches the analytical datasets and supports the following research steps [8,15–18].

However, recent studies [8,19–21] highlighted that a multi-scale approach based on the combination of "conventional" methods with advanced imaging techniques (*e.g.*, neutron and X-rays radiography and tomography) actually represents one of the best investigation option. The X-ray micro-computed tomography (μCT) is known to be a highly valuable analytical method to study the microstructure of stone materials [22], as it provides three-dimensional (3D) information with an excellent spatial resolution (down to the sub-micrometer scale) in a non-invasive way. Furthermore, it offers an overview of the 3D pore structure, including its modification in terms of morphological and quantitative parameters. In the last few years, the μCT has been widely used in conservation studies to investigate the relationship between the structure and the properties of building materials (stones, concretes [23], mortars [24–26]), their weathering/decay [9,27,28] and conservation [21,27,29–32].

The μCT studies can be carried out by using conventional X-rays sources as well as a synchrotron radiation (SR) source, the latter providing several advantages in terms of quicker acquisition time, better sensitivity and contrast, higher voxel size resolution and a general reduction of image artifacts [33]. The synchrotron radiation X-ray micro-computed tomography (SR-μCT) is potentially a powerful tool to study the effects induced by inorganic consolidating treatments on the stone microstructure, as they penetrate by capillarity in the pore network, impregnate the voids and modify the 3D pore system at the microscale [30]. It follows that, thanks to the high SR-μCT voxel size resolution (generally down to 1-2 μm or lower), it is possible to investigate the evolution of objects (solids, voids) at the scale of the voxel size.

Here, the SR-μCT is used in combination with conventional methods, as determination of water absorption by capillarity and mercury intrusion porosimetry, to investigate the microstructural variations induced by phosphate-based consolidating treatments to the Noto limestone, a porous carbonatic lithotype used as ornamental stone for facades and sculptures in the south of Italy.

A critical comparison among these methods is discussed in order to evaluate their peculiarities and complementarities to address scientific questions in the field of conservation treatments applied to preserve porous stone materials.

2 Materials and methods

2.1 Materials

The Noto limestone is a calcarenite outcropping in the Val di Noto (south-eastern Sicily) and used as building stone for the elaborated Baroque monuments since ancient time [34–38]. Among the several varieties of porous limestones of the Iblean Plateau, the *Noto Yellowish Limestone* variety was selected for the study. It is a biomicrite [38] mainly made of calcite, with subordinate clay minerals, quartz and iron oxides, and high porosity (25-37 %) in the range of the micro-pores [37].

A set of freshly quarried prismatic specimens (50×50×20 mm) were treated by poultice with a 0.76 M DAP water solution (DAP CAS Number 7783–28-0, assay ≥ 99.0%, reagent grade; dry cellulose pulp MH 300 Phase, Italy; poultice ratio ~ 5:1 DAP solution: cellulose pulp). A poultice layer of about 1-1.5 cm was applied on the specimen surface and a sheet of Japanese paper was placed between the paper poultice and the stone surface, to prevent damages due to the sticking of the poultice after drying. During the treatment, the specimens were wrapped in a plastic film. After 2 h, the plastic film was removed and the specimens were left drying at room temperature for 24 hours with the poultice on top. The poultice was then removed and all the specimens were rinsed three times by immersion in MilliQ water and dried again.

2.2 Methods

A characterization was carried out by scanning electron microscopy coupled with energy dispersive X-ray spectrometer (SEM-EDS, JEOL 5910 LV with tungsten filament coupled EDS spectrometer IXRF-2000) and by X-ray powder diffraction (XRPD, Panalytical X'Pert PRO X-ray powder diffractometer equipped with a Cu-Kα radiation) to check the morphology and mineralogical composition, respectively, of the stone matrix before and after the DAP treatment.

126 Measurements of the water absorption by capillarity were carried out on the same specimens
127 before and after the DAP treatment, in order to explore the modification induced by the
128 treatment on the water uptake properties of the lithotype. The measurements, performed
129 accordingly with the European Standard UNI EN 15801:2010 [11], determine the water
130 absorption of the specimens in contact with deionised water through a multiple layer of about
131 1 cm of filter papers (specimens dried for 7 days at 60±2 °C before the investigations,
132 experiments at room temperature in sealed boxes, measurements at regular steps: 10, 20, 30,
133 60 min, and 2, 4, 5, 24 h). The gravimetric increase is expressed as amount of absorbed water
134 per surface unit Q (mg cm^{-2}), water absorption curves (Q over square root of the absorption
135 time) and capillary absorption coefficient CA (mg $(cm^2\sqrt{s})^{-2}$ [39].
136
137 Mercury intrusion porosimetry (MIP) is used to study the porosity of the lithotype and the
138 measurements were carried out with a Thermo Scientific mercury intrusion porosimeter
139 Pascal 140 + Pascal 240. MIP data are collected in the pore radii range 50-0.0037 μm (the
140 pressure can be varied 0.02 - 200 MPa), which comprises from mesopores to megapores
141 according to the IUPAC classification [40,41]. The volume resolution is 0.1 mm^3 and
142 accuracy > 0.2 %. The pores are then subdivided in 20 pore size classes to describe the pore
143 size distribution and to evaluate the influence of smaller classes of pores on the total open
144 porosity. The Student's t-test was carried out on MIP results to determine the degree of
145 similarity between the two datasets.
146 Due to the destructive nature of this technique (mercury impregnates the sample and a
147 complete removal of it after the investigation is not feasible; pressure exerted by mercury
148 porosimeter might occasionally generates spurious micro-cracks [23]), it was not possible to
149 repeat the MIP investigations on the same sample before and after the treatment; then, a first
150 set of 3 samples was analyzed to study the lithotype microstructure before the treatment and a
151 second group of 9 samples to highlight to modifications occurred after the crystallization.
152
153 Synchrotron radiation X-ray micro-computed tomography (SR-μCT) was used to investigate
154 the pore network and to explore the influence of DAP treatments on its 3D features. SR-μCT
155 investigations were carried out at the ID11 beamline of ESRF (European Synchrotron
156 Radiation facility; Grenoble, France). The hard X-ray imaging experiments were carried out
157 using a parallel monochromatic 25 keV X-ray beam. The samples were mounted onto a high-
158 resolution rotation stage and 1440 X-ray projections were acquired with constant angular step
159 over a 180° rotation, with a sample-to-detector distance of 80 mm (phase-contrast mode),

exposure time/projection 1.5 s and effective pixel size of 0.9 μm. The scintillator screen used to convert X-rays into visible light consists of a gadolinium oxysulfide layer of 60 μm thickness. The image on the scintillator was recorded with a Fast Readout Low Noise detector (FReLoN), equipped with a 14 bit dynamic CCD camera and a 2048×2048 pixel chip.

To reconstruct a 3D image of the specimens, the tomographic projections were elaborated with the *SYRMEP Tomo Project* (STP), an open-source software tool designed for post-beamtime use [42,43]. In order to enhance the reliability of morphological and quantitative analysis of porosity, a single-distance phase-retrieval algorithm was used to increase the contrast between solid portion and voids. The 2D reconstructed slices were pre- and post-processed by using the ImageJ freeware software [44,45].

The segmentation (or binarization) of digital images was carried out in order to distinguishing elements of the stone matrix (voids, calcite of the substrate, newly-formed phases), initially detectable by their different grey values. During the process, the use of suitable thresholds allowed to isolate the voids from the stone matrix and provided an estimation of the total porosity. The segmentation resulted into binary images where similar elements are visualized as sets of contiguous voxels. Filtering has been necessary to homogenize the images, to enhance the contrast, to reduce the background noise of the reconstructed slices (which might negatively affect the segmentation process) and to enhance the pores borders of the original volume stacks [46,47].

The connected porosity was extracted from the segmented images using the tool "Find connected regions" of the FIJI software. Isolated pores were extracted by the total porosity by subtraction and separately analyzed.

The quantitative 3D image analysis of the porosity was carried out with the software library *Pore3D* [46].

In order to analyze the basic textural features of the pore structure and the connectivity of the pores, the following quantitative morphometric parameters of *Minkowskii functionals* were obtained: i) the volume density (V_v), a dimensionless parameter ($0< V_v <1$) expressed as the ratio of the number of voxels belonging to the object phase with respect to the total number of voxels in the considered VOI. In this study, the object phase is the pores, thus V_v corresponds to the porosity; ii) the Euler characteristics (X_v), a descriptor index of the connectedness of a 3D pore network, indicating the number of connections between void structures per unit volume. X_v is expressed in mm^{-3} and it is positive when the number of

isolated pores exceeds the number of multiple interconnections between the pores or negative for connected pore networks [48].

Several volume of interest (VOI) were selected assuming that the VOI is big enough to enclose a representative amount of the sample heterogeneity (Representative Elementary Volume, REV) [46,49]. The REV size was determined by using the box-counting method [50], namely by studying the variation of the volume density for multiple concentric increasing sub-volumes (Fig. 1a) and calculating the variability at each step in the form of a dimensionless coefficient of variation *Cv* (arithmetic mean divided by the standard deviation) [51]. In this study, representative 3D subvolumes of 300×300×300 voxels each (corresponding to a cube of ~300 µm side length) are initially extracted from the original dataset, considering the criterion suggested by Zhang et al. [52], which defines the REV on the basis that the mean reaches a reasonable plateau ($Cv < 0.2$) as shown in Fig. 1b.

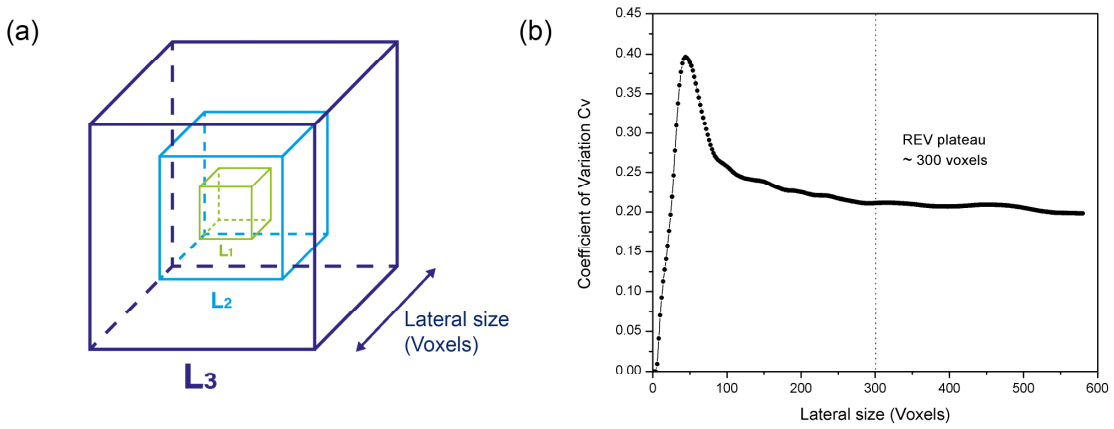

Fig. 1 (a) scheme, not in scale, of the REV size determination by using the box-counting method [46,49]. The volume density (*Vv*, the ratio of the number of voxels belonging to the voids with respect to the total number of voxels in the considered VOI) is the investigated variable to determine the REV. (b) REV determination by plotting the coefficient of variation *Cv*, defined as the ratio of the arithmetic mean divided by the specimen standard deviation, vs. the lateral size, a progressive and concentric number of voxels. A reasonable plateau is reached for cubes of about 300 voxels per side

Skeletonization, a thinning procedure for a simpler visualization of the "backbone" of the pore object, was carried out on the connected pores by applying the GVF algorithm [48,53]. As the skeletonization preserves the geometrical and morphological feature of the pore object, the skeleton and its 3D volumes are used to investigate and visualize the actual connectivity of the pore network.

The 3D renderings were obtained using the commercial software VGStudio 3.1.2.

SR-μCT investigations were not carried out on the same specimen before and after the consolidation as small samples (2×2×20 mm) are required in order to collect high resolution datasets.

For these reasons, suitable fragments for MIP (7×7×2 mm) and SR-μCT (2×2×20 mm) were sampled from the 50×50×20 mm specimens, before and after the DAP treatment. This condition does not negatively affect the study, which is aimed at obtaining an overview of the porous network modification trend induced by the treatment to the stone matrix

MIP and SR-μCT investigations are referred to the first 2 millimetres of the treated surface, as the crystallization and the microstructure modification was found to be more apparent in the portion of material closer to the treated surface (unpublished data).

3 Results

The reaction of DAP water-based solutions with calcite of Noto limestone promotes the crystallization of calcium phosphates on pore walls, as assessed by the morphological observations and by the elemental distribution of calcium and phosphorus (Fig. 2a-c). In particular, the untreated lithotype shows neat grain boundaries, whereas the treated matrix exhibits a crystal growth in dark grey values at the interface between the pores walls and the voids. The newly-formed phases are calcium phosphates as revealed by the EDS microanalyses of Fig. 2c, which display the well distinguishable formation of the Ca- and P-bearing phases on the boundaries of calcite grains. The XRD analyses allow associating the morphological features observed by SEM-EDS to the nature of the new phases, which are mainly composed of poorly crystalline hydroxyapatite (X-ray diffraction peaks at ~ 3.43 Å (002), 2.77 Å (112), 1.71 Å (004), Fig. 2d) mixed with a lower faction of other calcium phosphates (*i.e.*, octacalcium phosphate, poorly crystalline ion-substituted apatite; the potential composition of these phases has recently been discussed in the recent literature [4,7,54,55].

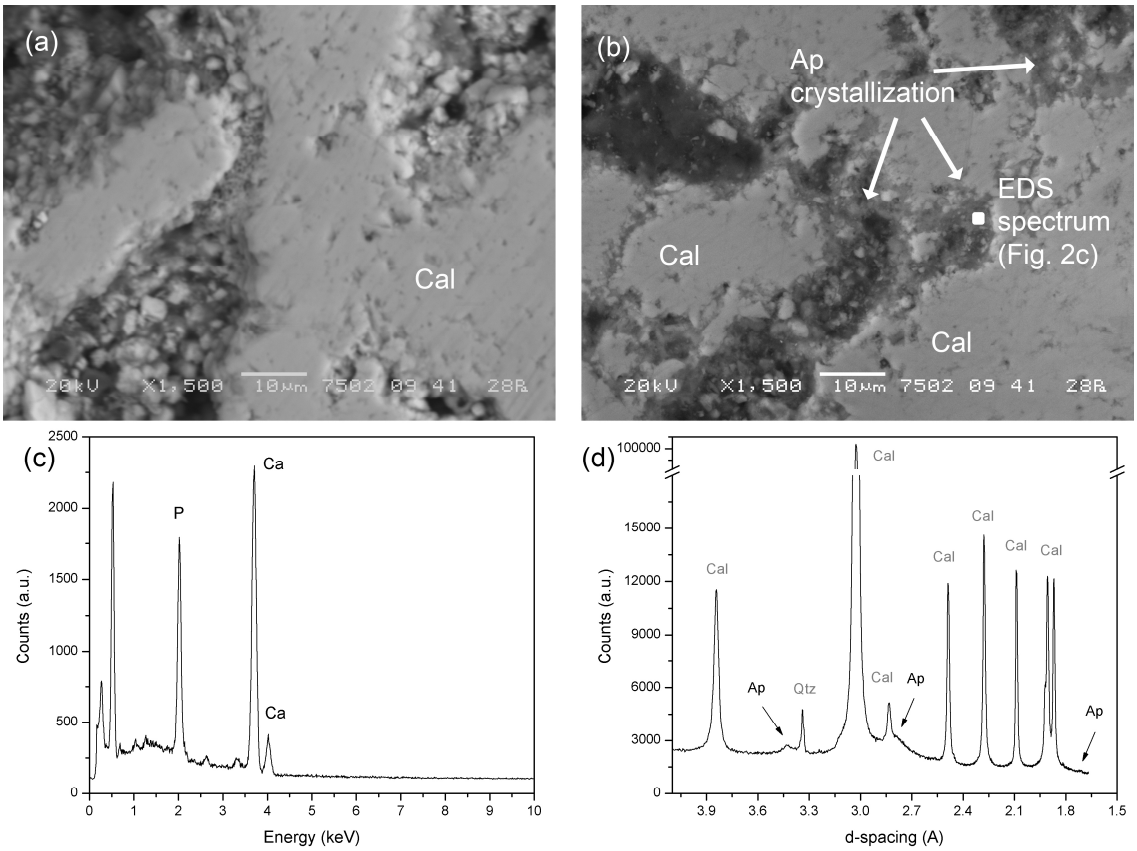

Fig. 2 SEM images of untreated (a) and treated (b) Noto limestone. In (a) the grain boundaries of calcite are neat while in (b) the pore walls show irregular boundaries and the overgrowth of newly-formed phases in darker grey value (pointed out by the arrows). The EDS microanalyses showed in (c) is carried out on a representative dark grey area of the (b) image and displays the well distinguishable formation of the Ca- and P-bearing phases on the boundaries of calcite grains. XRD pattern of the treated Noto limestone (d). Cal = calcite, Qtz = quartz, Ap = apatite and calcium phosphates

3.1 Water absorption by capillarity

A comparison of the water absorption curves of Noto limestone specimens before and after the DAP-based consolidation is plotted in Fig. 3, as the average of the measurements carried out on 6 specimens. A modification after the application of the treatment is unambiguously detected: the Q values (amount of water absorbed per surface unit, mg cm^{-2}) decrease after the DAP treatment at each absorption time. At the end of the measurements, the treated specimens show a total Q slightly lower than in the untreated specimens.

The capillary absorption coefficient CA (the curve slope) shows that the almost complete saturation of the specimens is slower after the treatment. In fact, the plateau of the curve is

reached in 35-42 √s (~ 20-30 min) in the untreated stone and in 60 √s (~ 60 min) in the treated one.

The variation of the sorptivity properties is correlated to the porosity modification, which in turn depends on the DAP reaction with calcite of pore walls. To explore these changes, the microstructure and the 3D pore system are investigated by MIP and SR-µCT.

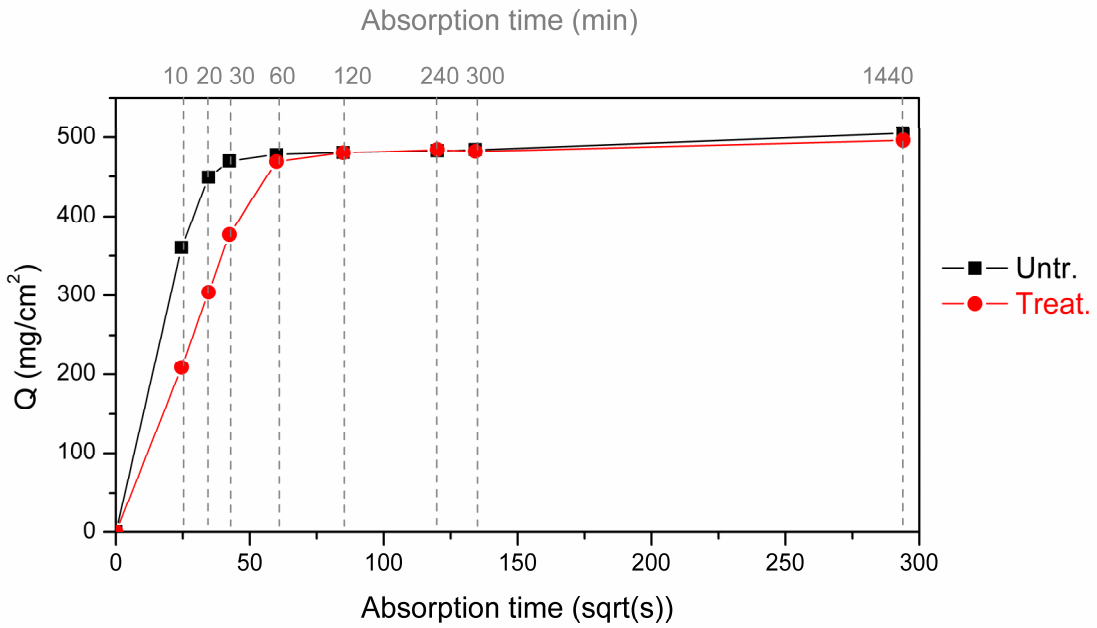

Fig. 3 Water absorption curves of untreated (-■- Untr.) and treated (-●- Treat.) Noto limestone specimens. Each curve is the average of the water absorptions of 6 different specimens. Time is expressed also in minutes (min) for clarity's sake. All the treated specimens undergo a similar trend, namely, the decrease of the suction speed and the fraction of water absorbed in the short term

3.2 Mercury intrusion porosimetry (MIP) measurements

The results of mercury intrusion porosimetry measurements of untreated and treated Noto limestone are showed in Fig. 4. The MIP data, their standard deviation and the results of the Student's t-test are given in the Appendix A.

The untreated Noto limestone is characterized by an average total open porosity between 36.05 % (standard deviation σ = 1.17 %), which is in agreement with the values assessed in a previous study carried out on a even wider set of quarry specimens [35,37]. Its pore size distribution is characterized by an unimodal feature with the ~70 % of the total open porosity in the range of 7.5-1.0 µm, while the remaining total open porosity is partitioned as following: about 18-19 % of the pores have a pore radius range between 1-0.1 µm, 6-7 %

have a pore radius lower than 0.1 μm and about 5-6 % have a pore radius larger than 7.5 μm. The average pore radius is 2.49 μm (σ = 0.36 μm).

The treated lithotype shows a different feature, with the average of the total open porosity of 33.62 % (σ = 2.99 %) and an average pore radius of 1.67 μm (σ = 0.38 μm).

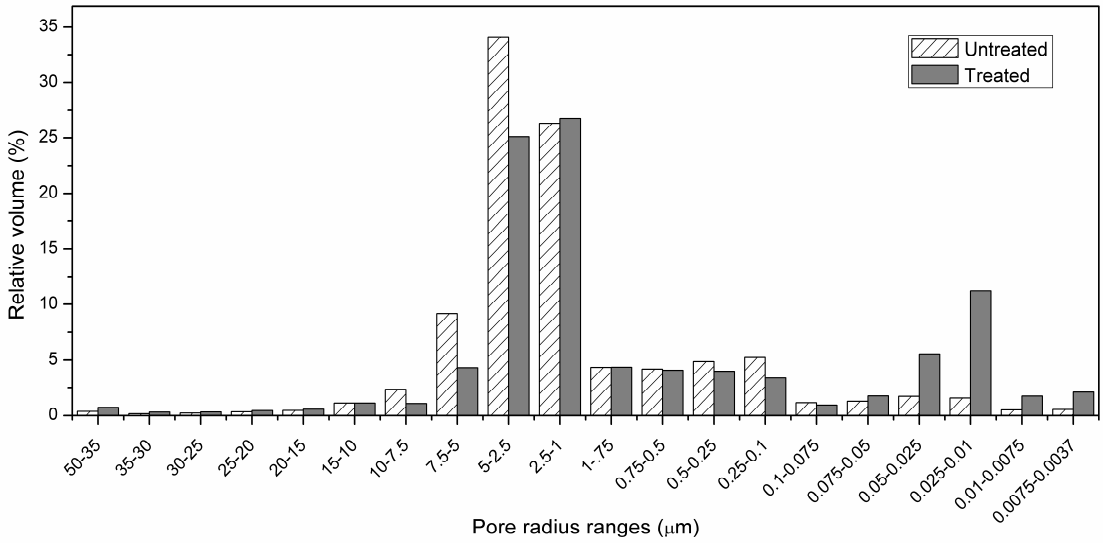

Fig. 4 Pore size distribution of Noto limestone before (Untreated) and after (Treated) the DAP consolidating treatment. The histograms are the average of 3 and 9 specimens for the untreated and treated lithotype, respectively

As for the pore size distribution, the treated stone specimens show differences with respect the untreated ones: i) the average pore radius is about 26-33 % thinner; ii) the percentage of coarser pores is lower, especially those having radius in the range 15-2.5 microns, while the percentage of finer ones (voids characterized by radius smaller than 1 μm) is higher.

Statistically, a significant difference on the average pore radius and on the pore size distribution between untreated and treated specimens has been observed, as demonstrated by their standard deviation and by the low probabilities calculated by the Student's t test (for average pore radius: $p = 0.01$; for pores with radius smaller than 0.5 μm: $0.00 \leq p \leq 0.23$, Student's t test; complete data available in the Appendix A). Differences on the total open porosity ($p = 0.21$, Student's t test) have been also recorded, even though the DAP treatment contribute is most likely partially blinded by the microstructural heterogeneity of the lithotype.

3.3 Synchrotron radiation X-ray micro-computed tomography (SR-μCT)

The two external slices, the selection of a representative VOI and the descending volume rendering of untreated and treated Noto limestone are shown in Fig. 5. In the slices of untreated Noto limestone, mainly two grey values are visible: a dark grey, corresponding to the voids of the sample, and a lighter one, corresponding to calcite crystals of the matrix. The slices of treated Noto limestone show a different morphology, with a third halfway grey value chiefly localized inside the pores and on pore walls, most likely composed by micro-particles; this suggests a correlation between this third grey value to the formation of micrometric and sub-micrometric phases. These morphologies are very similar to those observed by SEM on an equivalent treated specimen (Fig. 2b).

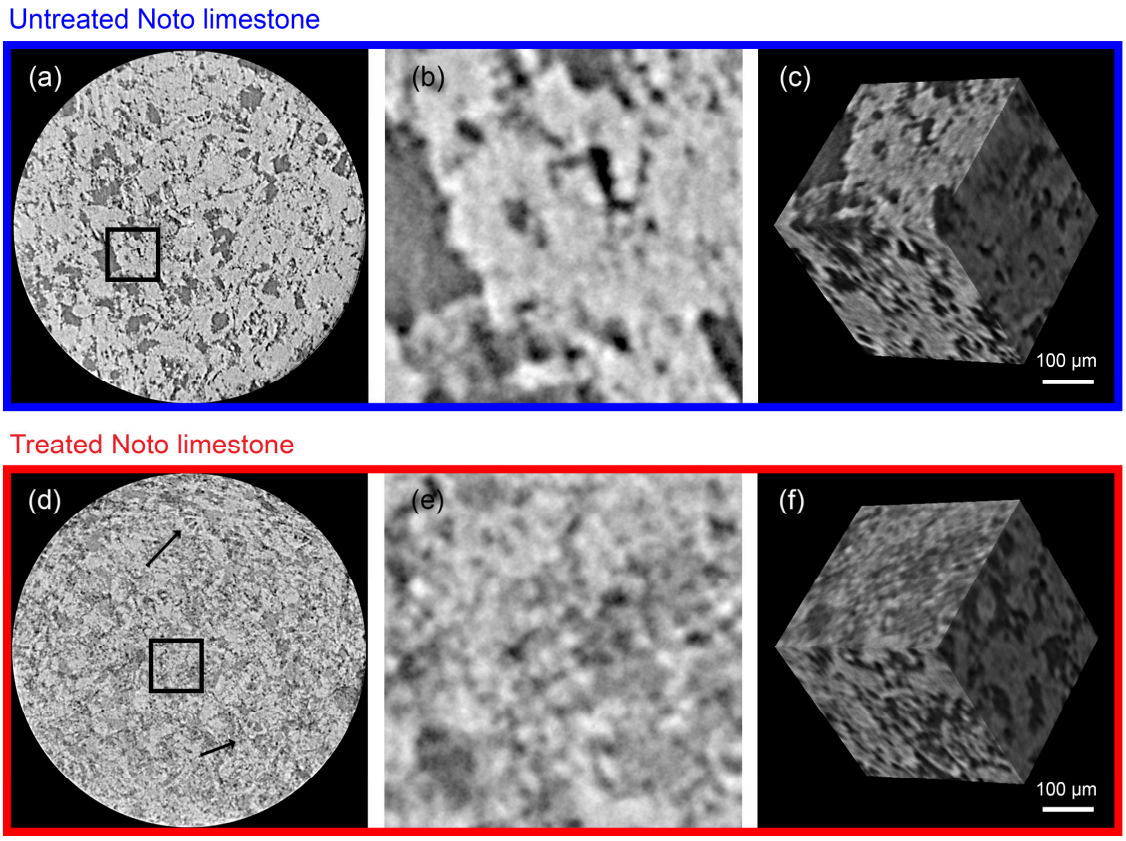

Fig. 5 Untreated and treated Noto limestone. Reconstructed slice of the surface (a, d), detail of an area of 300x300 voxel^2 indicated by the black square (b, e) and volume renderings (c, f)

The crystallization appears more visible in the most external slices (closer to the treated surface), whereas it wanes reaching the inner slices. This feature reverses in the last slices, where the image reconstruction shows a further increase of halfway grey values attributed to phosphates in the voids. This can be attributed to a more abundant crystallization of new phases, which most likely occurs locally, in correspondence of preferential diffusion path. SR-μCT images demonstrated that the new phases do not fill the voids but form a highly porous network of micrometric crystals nucleated on the pore surfaces.

In order to study the pore distribution and connectivity, the voids were digitally isolated from the bulk of the stone matrix by segmentation. In this SR-μCT study, the total porosity estimated during the thresholding is ~24.91 % for untreated Noto limestone and ~22.79 % for the treated sample. As calculated by the morphometric analysis, about the ~95-96 % of the total porosity is composed by a system of open and interconnected cells (connected porosity), while the remaining fraction are isolated voids (Table 1, presented as volume density V_v). The treated stone material shows a slightly higher percentage of connected pores with respect to the untreated one, even though the difference is rather negligible. The datasets generated by the segmentation of the voids on untreated and treated Noto limestone are showed in Fig. 6 and Fig. 7 as 3D renderings of interconnected and isolated pores.

Table 1 Morphometric analysis. The arithmetic mean (AM) and the standard deviation (σ) are indicated for values obtained with the morphometric analysis

Feature of the VOI		**Sample**	
		Untreated Noto limestone	**Treated Noto limestone**
Volume of total voids (%)		~24.91	~22.79
Volume density V_v of connected pores	AM	0.26	0.20
	σ	0.03	0.02
Volume density V_v of isolated pores	AM	0.008	0.007
	σ	0.0009	0.002
Euler characteristics X_v of connected pores (mm^{-3})	AM	-22583	-28549

	σ	12094	9537

346

347

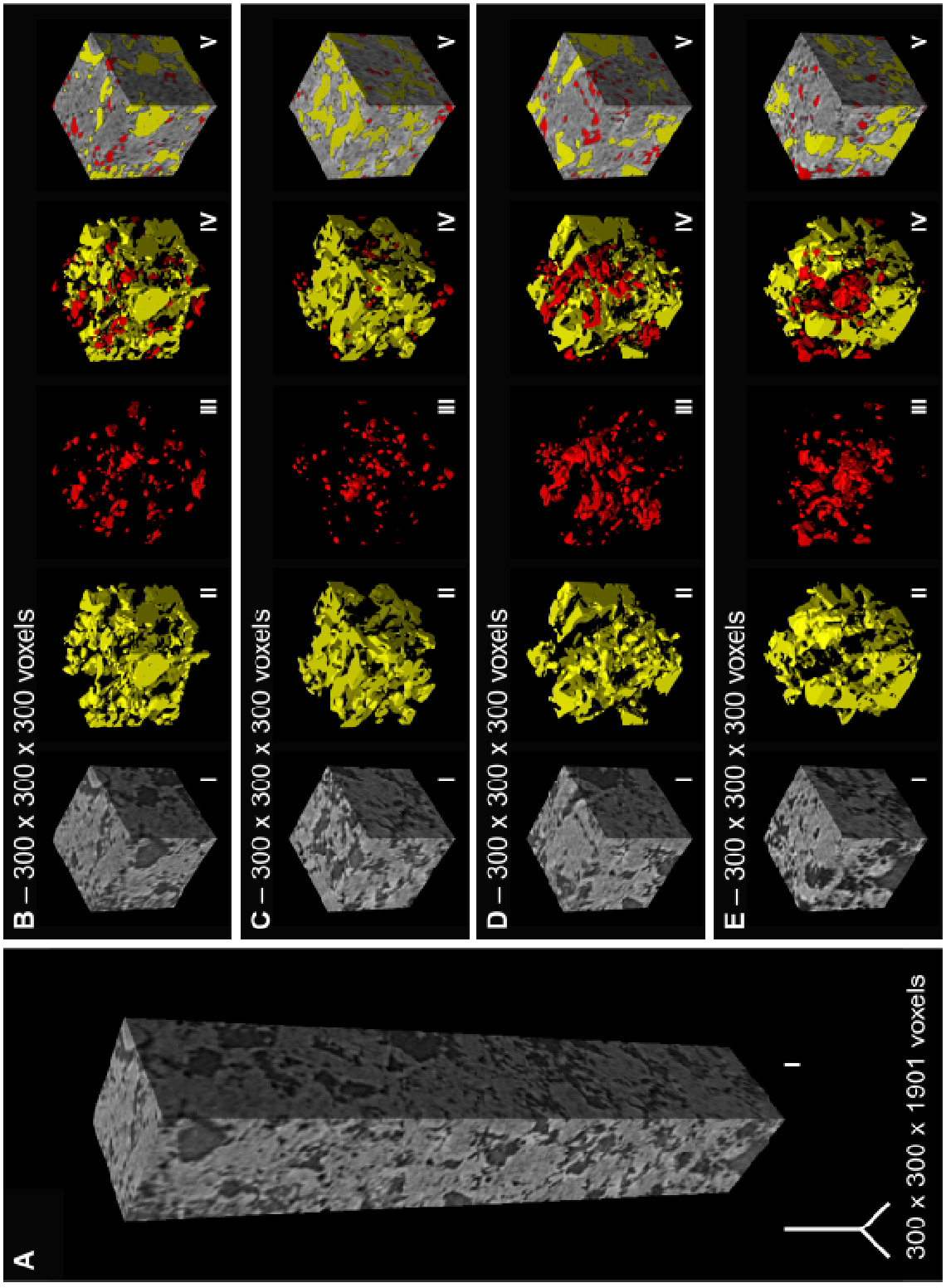

Fig. 6 Volume renderings of untreated Noto limestone: parallelepiped cropped from the whole SR-μCT dataset (A) and VOIs (300×300×300 voxels) close to the surface (B), just below (C), from the middle (D) and close to the bottom (E). The renderings include: X-ray tomographic images (I), connected (II) and isolated (III) pores, combination of connected and isolated pores (IV) and their inset in the volume rendering

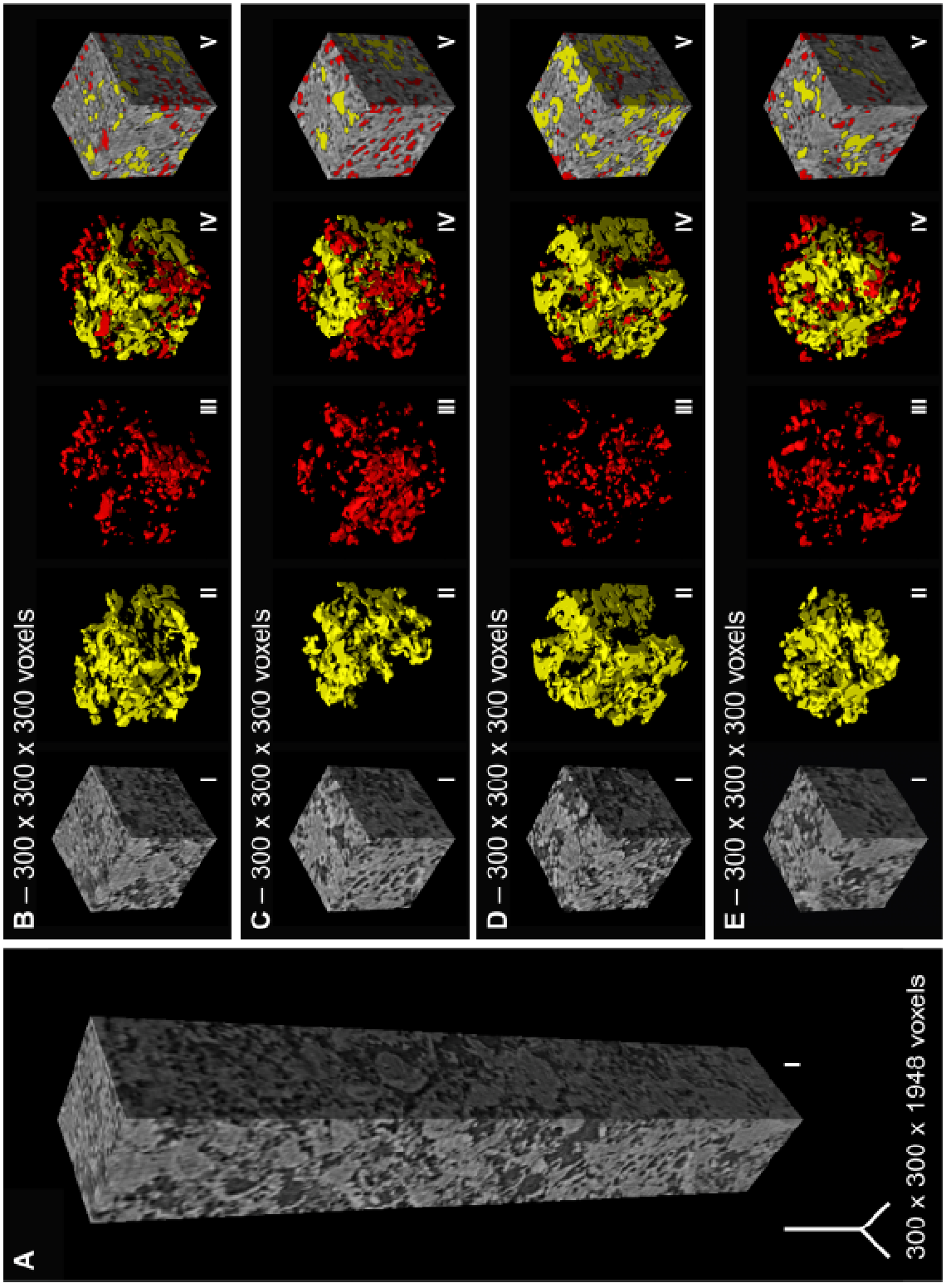

Fig. 7 Volume renderings of treated Noto limestone: parallelepiped cropped from the whole SR-μCT dataset (A) and VOIs (300×300×300 voxels) close to the surface (B), just below (C), from the middle (D) and close to the bottom (E). The renderings include: X-ray tomographic images (I), connected (II) and isolated (III) pores, combination of connected and isolated pores (IV) and their inset in the volume rendering

No cracks are detected, indicating that: i) the quarry lithotype used in this study does not exhibit natural discontinuities; ii) the crystallization of new phases within the matrix during the treatment does not introduce a mechanical stress to the microstructure, which in turn might generate cracks.

Focusing on the connected components, the so-called "open porosity", the porous structure of all the VOIs is characterized by a complex system of branching. The image processing of connected regions, namely regions composed by contiguous voxels in at least one of the three direction (threshold used: 10000 voxels, connection with face-face, side-side or corner-corner), revealed that the porous structure is highly interconnected and that there is a low number of connected pores in all the investigated VOIs. In many VOIs, one, two or three "objects" (namely, pores) constitute a single highly branched void of a determined VOI. In other words, selecting a single and even small pore, its branching constitutes a relevant % of the total open porosity of the investigated volume. This feature is present either on the untreated matrix or on the treated one.

The high connectivity of the Noto limestone microstructure is explored by the quantitative morphometric analysis, by the features extracted from the skeleton analysis [48] and by its 3D renderings (Fig. 8).

The Euler characteristics (X_v), used as topological descriptors and calculated on binarized volumes, are shown in Table 1. The X_v values are negative either before or after the DAP treatment, thus demonstrating that the pores of both the stone matrixes are highly interconnected. The treated lithotype is characterized by more negative X_v values than those recorded on the untreated one, indicating that the treated matrix has a more interconnected porous framework than the untreated one. This aspect could be an effect induced by the DAP treatment, even though it is not possible to attribute this feature only to the consolidation as the investigations are carried out on different micro-specimens, which are highly heterogeneous.

The skeleton analyses confirm the high connectivity of the pore network, showing that the branching of the pore space is composed by an open cell structure linked by a high number of connecting channel. Fig. 8 shows an isosurface rendering of the stone matrix of treated Noto limestone, with the inset of the skeleton and the volume rendering of the max spheres inflated in the nodes of the skeleton. The nodes are the "pore bodies" [48], namely the junction voxels among three or more branches. The connected pores are represented by the skeleton and they compose a dense framework of branches mutually interconnected.

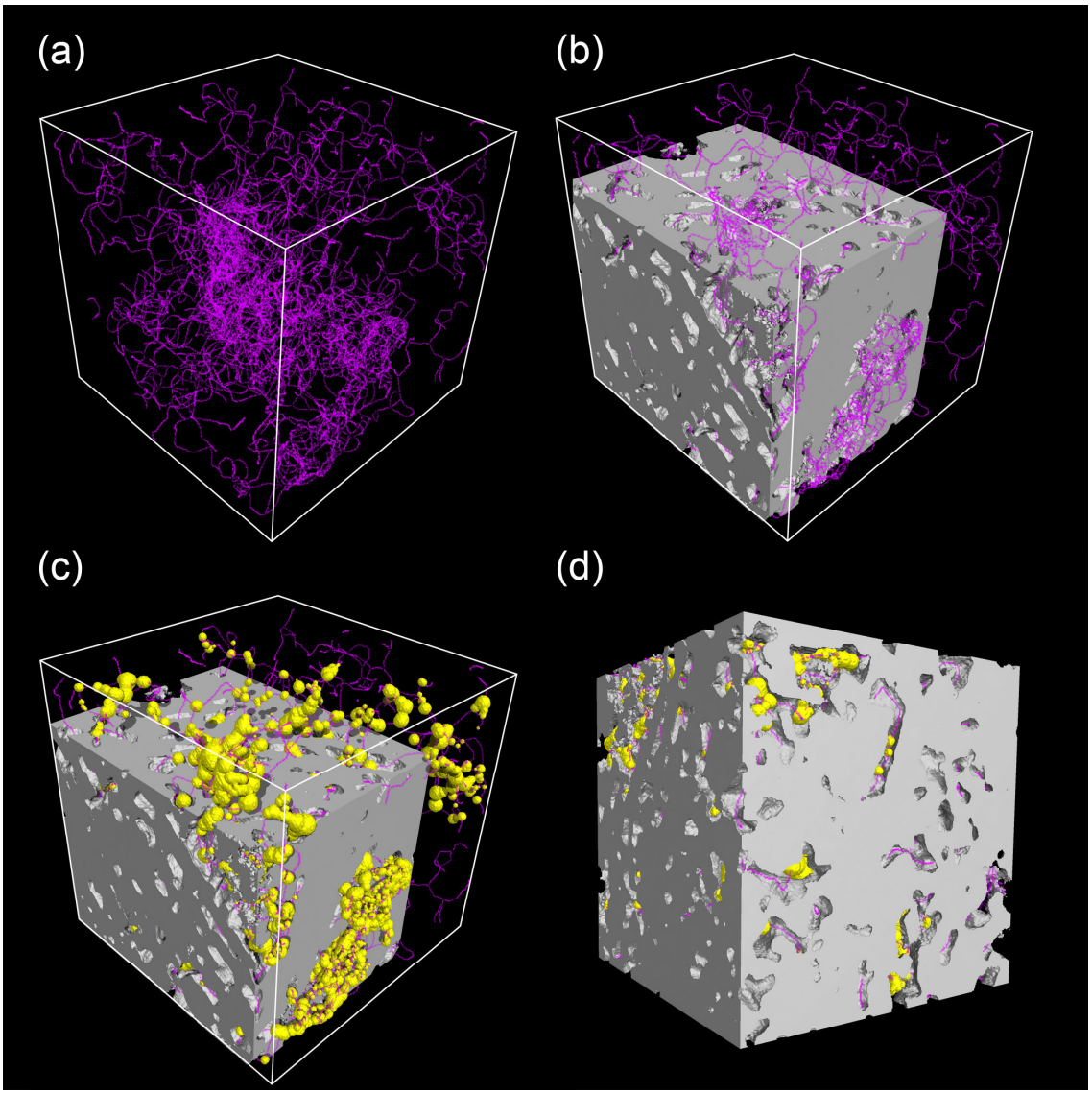

Fig. 8 3D rendering of the connected pores skeleton (in violet) of treated Noto limestone (a). The white cube represents the VOI of 300×300×300 voxels; inset of the skeleton in a clipped isosurface rendering of the VOI (b); pore nodes (in yellow) of the skeleton, namely the volume rendering of the max spheres inflated in the nodes of the skeleton (c). The nodes are the "pore bodies", namely the junction voxels among three or more branches; 3D rendering of the VOI with the inset of pore nodes and skeleton without clippings.

4 Discussion

The water absorption measurements show evidence that the stone matrix preserves its wetting and hydrophilic properties after the DAP consolidating treatment. At the same time, the stone material exhibits a decrease in the amount of water uptake per surface unit and of the suction speed. This effect is related to a modification of the microstructure of the material, due to the

crystallization of newly-formed phosphate phases on pore walls. In fact, the treated Noto limestone specimens show evidence of a minor total open porosity, a minor average pore radius and a different pore size distribution with respect to the untreated matrix. It is conceivable that these differences depend on the DAP consolidating treatment: in particular the variation of the average pore radius and the pore size distribution, where the standard deviation of MIP measurements was pretty narrow and the statistical t-test results showed noticeable differences.

The crystallization of the new phases within the stone matrix and the descending microstructural effects are univocally attributed to the diffusion itself and not to a system of micro-cracks which might acts as preferential diffusion paths. Both before and after the DAP treatment, the stone matrix is characterized by a system of highly interconnected communicating channels, which is the "spine" that rules to the consolidant impregnation and redistribution.

The MIP contribute is essential for the exploration of the sub-micrometric pore classes (micropores IUPAC range) variations, even though approximated to a system of cylinder-shaped capillaries. On the other side, SR-μCT volume renderings showed that in many cases the pores are quite different from an idealized system of cylinders, as their morphology frequently presents throats, bigger pores connected by thinner channels, pore-to-end branches, irregular-shaped cavities, etc. For these reason, SR-μCT investigations allowed visualizing and quantifying the actual morphology of the voids (within the resolution limit), bypassing the cylinder-shaped model used by MIP (which, as drawback, suffers of the ink-bottle effects and is subjected to the overestimation of finer pores).

The MIP and the SR-μCT results comply with the finding that the total open porosity is higher in the treated lithotype than in the untreated one, even though the SR-μCT porosity values are different from MIP ones. The discrepancy of the porosity values for the same type of specimen is due to several reasons, mainly the different "resolution" of the two techniques. In fact, the μ-CT datasets of this study have a maximum voxel size of 1 μm^3, whereas the used porosimeter is able to measure pores down to 0.0037 μm of radius. This means that with μ-CT it is possible to detect pores with a diameter of at least 1 μm, while with MIP of at least 0.0074 μm. Therefore, a part of the open porosity of Noto limestone, treated and untreated, is below the detection limit of SR-μCT and all the pore objects with a size minor than 1 μm^3 are not detectable. Considering for example the total open porosity of the untreated Noto limestone (~36 %) and excluding all the pore classes detected by MIP and not detectable by

μ-CT (classes with pore diameter < 1 μm, about ~6.5 %), the MIP porosity decreases from ~36% to ~29.5%.

On the other hand, it should be considered that the μ-CT porosity values (e.g., the ~25 % for the untreated Noto limestone) is slightly underestimated because the volume % is calculated by the software using threshold algorithms and image filters, thus differences in the calculated volume % of voids might rise by varying the threshold values and by changing the algorithm and the filters. In addiction, considering that at least two or three contiguous voxels are needed to be identified as a void and not as noise, pores with a radius minor than 1 μm cannot be considered in the total porosity quantified by SR-μCT. Without using any filter and considering spurious voxels as possible pores, the porosity measured by μ-CT ranges between 27-30 %, which is close to the MIP values (29.5%).

Moreover, further elements should be also considered, as the micro-heterogeneity of the lithotype, the impossibility to carry out MIP and μ-CT investigations on the same sample (due to the intrinsic limitation of the techniques), the pore size distribution (assessed by MIP) of the treated lithotype which is different from the untreated one, with a % volume decrease of the pore classes detectable by SR-μCT and a % volume increase of not detectable voids.

Last but not least and focusing on the new properties of the treated stone, the crystallization of phosphate phases on the profile of calcite grains and on pore walls modifies the microstructure of the lithotype and increases the volume occupied by solid phases. It is conceivable that the crystallization within the stone matrix also reconnects detached stone grains and/or incoherent micro-elements, and all these processes increase the cohesion of the stone microstructure. In addition, the consolidating phases (mainly poorly crystalline hydroxyapatite, mixed with other minor phases [4,7,54,55]) are characterised by a low solubility in water, even in acid environments (e.g., dissolution caused by acid rains, [56]), and it has a preventive action on the treated system with the inhibition of corrosion phenomena.

Conclusions

The evolution of microstructure and capillarity property of Noto limestone consolidated with DAP treatments have been investigated. The results highlight that the crystallization of phosphates within the stone matrix modifies the internal microstructure of the original lithotype, leading to a modification the properties of the stone matrix. At the same time, the

469 treatment does not revolutionize the lithotype in its peculiar features (*e.g.,* hydrophilic
470 properties, permeability to water flow, capability to absorb water by capillarity), which
471 actually experiences positive modifications in terms of suction speed. These variations are
472 expected to give positive implication mainly in outdoor conditions, where a minor capacity to
473 absorb water might preserve the stone material by the quick absorption of harmful water-
474 based solutions (*e.g.*, acid rains or rising of soluble salts solutions).
475 The combination of water absorption measurements with MIP and SR-μCT resulted to be a
476 powerful multi-analytical and multiscale approach to study the 3D textural feature of porous
477 stone materials and to understand how these materials are modified when treated with
478 inorganic-mineral products. In particular, the investigations carried out by SR-μCT
479 demonstrated the high potentiality of the technique to evaluate the effects (in terms of total
480 porosity, morphology, localization and connectivity) of the consolidating treatment on the
481 pore network. On the other side, the MIP measurements provide porosity data down to a sub-
482 micrometric scale, allowing to investigate the porosity and the pore size distribution for pore
483 classes whose detection is not permitted by SR-μCT.
484 The obtained results might elucidate the formation mechanism of the new phases inside the
485 pores and we are currently investigating the morphology of the stone boundaries among the
486 "calcite phase", the "void phase" and the "phosphate phase" after the DAP reaction, the
487 diffusion of the new phases within the stone matrix and their arrangement in cavities and on
488 the pore walls. By using the multiscale approach described in this study, the investigation of
489 the effects induced by different consolidating treatments to stone materials could provide
490 practical indications for the consolidant application in the restoration worksites. In this view,
491 the present study opens the scenario to new set of multi-scale studies focused to explore with
492 a high resolution a wide spectrum of porous geomaterials treated with innovative
493 conservation products.
494

495 ## Acknowledgements

496 The authors gratefully acknowledge the ESRF (European Synchrotron Radiation facility;
497 Grenoble, France) and the ID11 beamline for beamtime allocation (proposal n° MA3118), the
498 beamline scientist Dr. Jonathan Wright for his support in data acquisition and Dr. Roberta
499 Possenti for her support in the image processing.
500

Declaration of interest

None

Funding

This research did not receive any specific grant from funding agencies in the public, commercial, or not-for-profit sectors.

Supplementary information

Electronic supplementary material: The online version of this article contains supplementary material, which is available to authorized users (Appendix A).

Data availability

The raw/processed data required to reproduce these findings cannot be shared at this time as the data also forms part of an ongoing study.

References

[1] Commisione Tecnica UNI, UNI 11182:2006 Beni culturali - Materiali lapidei naturali ed artificiali - Descrizione della forma di alterazione - Termini e definizioni, (2006) 1–33.

[2] ICOMOS-ISCS, Illustrated glossary on stone deterioration patterns. English-French version, (2008) 1–78.

[3] G. Graziani, E. Sassoni, G.W. Scherer, E. Franzoni, Phosphate-based treatments for consolidation of salt-bearing Globigerina limestone, in: IOP Conf. Ser. Mater. Sci. Eng., 2018: p. 12082. doi:10.1088/1757-899X/364/1/012082.

[4] E. Possenti, C. Colombo, C. Conti, L. Gigli, M. Merlini, J.R. Plaisier, M. Realini, D. Sali, G.D. Gatta, Diammonium hydrogenphosphate for the consolidation of building materials. Investigation of newly-formed calcium phosphates, Constr. Build. Mater. 195 (2019) 557–563. doi:10.1016/j.conbuildmat.2018.11.077.

[5] E. Possenti, C. Colombo, C. Conti, L. Gigli, M. Merlini, J.R. Plaisier, M. Realini, G.D. Gatta, Grazing incidence synchrotron X-ray diffraction of marbles consolidated with diammonium hydrogen phosphate treatments: non-destructive probing of buried minerals, Appl. Phys. A. 124 (2018) 383. doi:10.1007/s00339-018-1798-8.

[6] E. Sassoni, Hydroxyapatite and Other Calcium Phosphates for the Conservation of Cultural Heritage: A Review, Materials (Basel). 11 (2018) 557. doi:10.3390/ma11040557.

[7] E. Possenti, C. Colombo, D. Bersani, M. Bertasa, A. Botteon, C. Conti, P.P. Lottici, M. Realini, New insight on the interaction of diammonium hydrogenphosphate

conservation treatment with carbonatic substrates: A multi-analytical approach, Microchem. J. 127 (2016) 79–86. doi:10.1016/j.microc.2016.02.008.
[8] G. Graziani, C. Colombo, C. Conti, E. Possenti, E. Perelli Cippo, M. Realini, E. Sassoni, Neutron radiography as a tool for assessing penetration depth and distribution of a phosphate consolidant for limestone, Constr. Build. Mater. 187 (2018) 238–247. doi:10.1016/j.conbuildmat.2018.07.173.
[9] J. Dewanckele, T. De Kock, M.A. Boone, V. Cnudde, L. Brabant, M.N. Boone, G. Fronteau, L. Van Hoorebeke, P.J.S. Jacobs, 4D imaging and quantification of pore structure modifications inside natural building stones by means of high resolution X-ray CT., Sci. Total Environ. 416 (2012) 436–48. doi:10.1016/j.scitotenv.2011.11.018.
[10] UNI Ente Nazionale Italiano di Unificazione, UNI EN 15866: 2010, Conservation of cultural property–test methods–colour measurement of surfaces., (2010).
[11] Commisione Tecnica UNI, UNI EN 15801:2010 Conservation of cultural property – test methods – determination of water absorption by capillarity, (2010).
[12] C.- ICR, NORMAL 7/81 Natural Stones Test Methods: Determination of Water Absorption by Total Immersion, (1981).
[13] C.- ICR, NORMAL 29/88 Determination of Drying Index, (1988).
[14] J.D. Rodrigues, A.P.F. Pinto, D.R. da Costa, Tracing of decay profiles and evaluation of stone treatments by means of microdrilling techniques, J. Cult. Herit. 3 (2002) 117–125. doi:10.1016/S1296-2074(02)01172-X.
[15] E. Sassoni, G. Graziani, E. Franzoni, An innovative phosphate-based consolidant for limestone. Part 1: Effectiveness and compatibility in comparison with ethyl silicate, Constr. Build. Mater. 102 (2016) 918–930. doi:10.1016/j.conbuildmat.2015.10.202.
[16] G. Graziani, E. Sassoni, G.W. Scherer, E. Franzoni, Penetration depth and redistribution of an aqueous ammonium phosphate solution used for porous limestone consolidation by brushing and immersion, Constr. Build. Mater. 148 (2017) 571–578. doi:10.1016/j.conbuildmat.2017.05.097.
[17] E. Franzoni, E. Sassoni, G. Graziani, Brushing, poultice or immersion? The role of the application technique on the performance of a novel hydroxyapatite-based consolidating treatment for limestone, J. Cult. Herit. 16 (2015) 173–184. doi:10.1016/j.culher.2014.05.009.
[18] I. Osticioli, G. Botticelli, P. Matteini, S. Siano, R. Pini, M. Matteini, Micro-Raman analysis on the combined use of ammonium oxalate and ammonium phosphate for the consolidation and protection of carbonate stone artifacts, J. Raman Spectrosc. 48 (2017) 966–971. doi:10.1002/jrs.5150.
[19] C. Conti, C. Colombo, G. Festa, J. Hovind, E.P. Cippo, E. Possenti, M. Realini, Investigation of ammonium oxalate diffusion in carbonatic substrates by neutron tomography, J. Cult. Herit. 19 (2016) 463–466. doi:10.1016/j.culher.2015.12.005.
[20] M. Realini, C. Colombo, C. Conti, F. Grazzi, E. Perelli Cippo, J. Hovind, Development of neutron imaging quantitative data treatment to assess conservation products in cultural heritage, Anal. Bioanal. Chem. 409 (2017) 6133–6139. doi:10.1007/s00216-017-0550-0.
[21] S. Raneri, G. Barone, P. Mazzoleni, I. Alfieri, L. Bergamonti, T. De Kock, V. Cnudde, P.P. Lottici, A. Lorenzi, G. Predieri, E. Rabot, J. Teixeira, Multi-scale laboratory routine in the efficacy assessment of conservative products for natural stones, MethodsX. 5 (2018) 1095–1101. doi:10.1016/j.mex.2018.08.013.
[22] V. Cnudde, M.N. Boone, High-resolution X-ray computed tomography in geosciences: A review of the current technology and applications, Earth-Science Rev. 123 (2013) 1–17. doi:10.1016/j.earscirev.2013.04.003.
[23] V. Cnudde, A. Cwirzen, B. Masschaele, P.J.S. Jacobs, Porosity and microstructure

586 characterization of building stones and concretes, Eng. Geol. 103 (2009) 76–83.
587 doi:10.1016/j.enggeo.2008.06.014.
588 [24] N. Marinoni, M. Voltolini, L. Mancini, P. Vignola, A. Pagani, A. Pavese, An
589 investigation of mortars affected by alkali-silica reaction by X-ray synchrotron
590 microtomography□: a preliminary study, J. Mater. Sci. 44 (2009) 5815–5823.
591 doi:10.1007/s10853-009-3817-9.
592 [25] M. Voltolini, N. Marinoni, L. Mancini, Synchrotron X-ray computed
593 microtomography investigation of a mortar affected by alkali–silica reaction: a
594 quantitative characterization of its microstructural features, J. Mater. Sci. 46 (2011)
595 6633–6641. doi:10.1007/s10853-011-5614-5.
596 [26] N. Marinoni, M. Voltolini, M.A.T.M. Broekmans, L. Mancini, P.J.M. Monteiro, N.
597 Rotiroti, E. Ferrari, A. Bernasconi, A combined synchrotron radiation micro computed
598 tomography and micro X-ray diffraction study on deleterious alkali-silica reaction, J.
599 Mater. Sci. 50 (2015) 7985–7997. doi:10.1007/s10853-015-9364-7.
600 [27] V. Cnudde, P.J.S. Jacobs, Monitoring of weathering and conservation of building
601 materials through non-destructive X-ray computed microtomography, Environ. Geol.
602 46 (2004) 477–485. doi:10.1007/s00254-004-1049-5.
603 [28] V. Cnudde, T. De Kock, M. Boone, W. De Boever, T. Bultreys, J. Van Stappen, D.
604 Vandevoorde, J. Dewanckele, H. Derluyn, V. Cárdenes, L. Van Hoorebeke,
605 Conservation studies of cultural heritage: X-ray imaging of dynamic processes in
606 building materials, Eur. J. Mineral. 27 (2015) 269–278. doi:10.1127/ejm/2015/0027-
607 2444.
608 [29] S. Bugani, M. Camaiti, L. Morselli, E. Van de Casteele, K. Janssens, Investigation on
609 porosity changes of Lecce stone due to conservation treatments by means of x-ray
610 nano- and improved micro-computed tomography: preliminary results, X-Ray
611 Spectrom. 36 (2007) 316–320. doi:10.1002/xrs.976.
612 [30] V. Cnudde, J.-P. Cnudde, C. Dupuis, P.J.S. Jacobs, X-ray micro-CT used for the
613 localization of water repellents and consolidants inside natural building stones, Mater.
614 Charact. 53 (2004) 259–271. doi:10.1016/j.matchar.2004.08.011.
615 [31] S. Bugani, M. Camaiti, L. Morselli, E. Van de Casteele, K. Janssens, Investigating
616 morphological changes in treated vs. untreated stone building materials by x-ray
617 micro-CT, Anal. Bioanal. Chem. 391 (2008) 1343–50. doi:10.1007/s00216-008-1946-
618 7.
619 [32] M. Slavíková, F. Krejčí, J. Žemlička, M. Pech, P. Kotlík, J. Jakůbek, X-ray
620 radiography and tomography for monitoring the penetration depth of consolidants in
621 Opuka – the building stone of Prague monuments, J. Cult. Herit. 13 (2012) 357–364.
622 doi:10.1016/j.culher.2012.01.010.
623 [33] M. Parisatto, A. Turina, G. Cruciani, L. Mancini, L. Peruzzo, B. Cesare, Three-
624 dimensional distribution of primary melt inclusions in garnets by X-ray
625 microtomography, Am. Mineral. 103 (2018) 911–926. doi:10.2138/am-2018-
626 6216CCBYNCND.
627 [34] M.F. La Russa, G. Barone, C.M. Belfiore, P. Mazzoleni, A. Pezzino, Application of
628 protective products to “Noto” calcarenite (south-eastern Sicily): a case study for the
629 conservation of stone materials, Environ. Earth Sci. 62 (2011) 1263–1272.
630 doi:10.1007/s12665-010-0614-3.
631 [35] G. Alessandrini, A. Bocci, R. Bugini, D. Emmi, R. Peruzzi, M. Realini, Stone
632 materials of Noto (Siracusa) and their decay, in: 7th Int. Congr. Deterior. Conserv.
633 Stone, 1993: pp. 11–20.
634 [36] C. Urzì, M. Realini, Colour changes of Notos calcareous sandstone as related to its
635 colonisation by microorganisms, Int. Biodeterior. Biodegradation. 42 (1998) 45–54.

636 doi:10.1016/S0964-8305(98)00045-6.
637 [37] G. Barbera, G. Barone, V. Crupi, F. Longo, G. Maisano, D. Majolino, P. Mazzoleni, S.
638 Raneri, J. Teixeira, V. Venuti, A multi-technique approach for the determination of the
639 porous structure of building stone, Eur. J. Mineral. 26 (2014) 189–198.
640 doi:10.1127/0935-1221/2014/0026-2355.
641 [38] G. Barone, V. Crupi, F. Longo, D. Majolino, P. Mazzoleni, S. Raneri, J. Teixeira, V.
642 Venuti, Neutron radiography for the characterization of porous structure in degraded
643 building stones, J. Instrum. 9 (2014). doi:10.1088/1748-0221/9/05/C05024.
644 [39] R. Peruzzi, T. Poli, L. Toniolo, The experimental test for the evaluation of protective
645 treatments: a critical survey of the "capillary absorption index," J. Cult. Herit. 4 (2003)
646 251–254. doi:10.1016/S1296-2074(03)00050-5.
647 [40] K.S.W. et al. Sing, Reporting physisorption data for gas/solid systems with special
648 reference to the determination of surface area and porosity (Recommendations 1984),
649 Pure Appl. Chem. 57 (1985) 603–619. doi:10.1351/pac198557040603.
650 [41] J. Rouquerol, D. Avnir, C.W. Fairbridge, D.H. Everett, J.M. Haynes, N. Pernicone,
651 J.D.F. Ramsay, K.S.W. Sing, K.K. Unger, Recommendations for the characterization
652 of porous solids (Technical Report), Pure Appl. Chem. 66 (1994) 1739–1758.
653 doi:10.1351/pac199466081739.
654 [42] F. Brun, L. Massimi, M. Fratini, D. Dreossi, F. Billé, A. Accardo, R. Pugliese, A.
655 Cedola, SYRMEP Tomo Project: a graphical user interface for customizing CT
656 reconstruction workflows, Adv. Struct. Chem. Imaging. 3 (2017) 4.
657 doi:10.1186/s40679-016-0036-8.
658 [43] E. Larsson, Quantitative Analysis of Bone Tissue Engineering Scaffolds and Skull
659 Bones by means of Synchrotron and Conventional X-ray Computed Microtomography
660 Quantitative Analysis of Bone Tissue Engineering Scaffolds and Skull Bones by
661 means of Synchrotron and Conve, Link¨ oping University, 2010.
662 [44] M.D. Abramoff, P.J. Magalhães, S.J. Ram, Image processing with ImageJ,
663 Biophotonics Int. 11 (2004) 36–42.
664 [45] J. Schindelin, I. Arganda-Carreras, E. Frise, V. Kaynig, M. Longair, T. Pietzsch, S.
665 Preibisch, C. Rueden, S. Saalfeld, B. Schmid, J.-Y. Tinevez, D.J. White, V.
666 Hartenstein, K. Eliceiri, P. Tomancak, A. Cardona, Fiji: an open-source platform for
667 biological-image analysis, Nat. Methods. 9 (2012) 676–682. doi:10.1038/nmeth.2019.
668 [46] F. Brun, L. Mancini, P. Kasae, S. Favretto, D. Dreossi, G. Tromba, Pore3D: A
669 software library for quantitative analysis of porous media, Nucl. Instruments Methods
670 Phys. Res. Sect. A Accel. Spectrometers, Detect. Assoc. Equip. 615 (2010) 326–332.
671 doi:10.1016/j.nima.2010.02.063.
672 [47] M. Voltolini, D. Zandomeneghi, L. Mancini, M. Polacci, Texture analysis of volcanic
673 rock samples: Quantitative study of crystals and vesicles shape preferred orientation
674 from X-ray microtomography data, J. Volcanol. Geotherm. Res. 202 (2011) 83–95.
675 doi:10.1016/J.JVOLGEORES.2011.02.003.
676 [48] F. Brun, Development of algorithms and methods for three-dimensional image analysis
677 and biomedical applications, Universit` a degli Studi di Trieste, 2011.
678 [49] I.M. Gitman, H. Askes, L.J. Sluys, Representative volume: Existence and size
679 determination, Eng. Fract. Mech. 74 (2007) 2518–2534.
680 doi:10.1016/J.ENGFRACMECH.2006.12.021.
681 [50] M.S. Costanza-Robinson, B.D. Estabrook, D.F. Fouhey, Representative elementary
682 volume estimation for porosity, moisture saturation, and air-water interfacial areas in
683 unsaturated porous media: Data quality implications, Water Resour. Res. 47 (2011)
684 2893–900. doi:10.1029/2010WR009655.
685 [51] M. Zambrano, E. Tondi, L. Mancini, F. Arzilli, G. Lanzafame, M. Materazzi, S.

686 Torrieri, 3D Pore-network quantitative analysis in deformed carbonate grainstones,
687 Mar. Pet. Geol. 82 (2017) 251–264. doi:10.1016/j.marpetgeo.2017.02.001.
688 [52] D. Zhang, R. Zhang, S. Chen, W.E. Soll, Pore scale study of flow in porous media:
689 Scale dependency, REV, and statistical REV, Geophys. Res. Lett. 27 (2000) 1195–
690 1198. doi:10.1029/1999GL011101.
691 [53] F. Brun, D. Dreossi, Efficient curve-skeleton computation for the analysis of
692 biomedical 3D images, Biomed. Sci. Instrum. 46 (2010) 475–480.
693 [54] E. Possenti, Inorganic products used in the Conservation of Cultural Heritage:
694 interaction with carbonatic substrates and newly-formed crystalline phases, University
695 of Milan, 2019.
696 [55] E. Possenti, C. Conti, G.D. Gatta, M. Realini, C. Colombo, Diammonium
697 Hydrogenphosphate Treatment on Dolostone: the Role of Mg in the Crystallization
698 Process, Coatings. 9 (2019) 169. doi:10.3390/coatings9030169.
699 [56] G. Graziani, E. Sassoni, G.W. Scherer, E. Franzoni, Resistance to simulated rain of
700 hydroxyapatite- and calcium oxalate-based coatings for protection of marble against
701 corrosion, Corros. Sci. 127 (2017) 168–174. doi:10.1016/j.corsci.2017.08.020.
702